Journal of Computational and Applied Mathematics 259 (2014) 955–964

Contents lists available at ScienceDirect

Journal of Computational and Applied Mathematics

journal homepage: www.elsevier.com/locate/cam

Lagrangian based mathematical modeling and experimental validation of a planar stabilized platform for mobile systems ☆

Babak Rohani [a], Yigit Yazicioglu [a], Mehmet Mutlu [b,*], Orkun Ogucu [b], Emre Akgul [b], Afsar Saranli [b]

[a] Middle East Technical University, Department of Mechanical Eng., Ankara, Turkey

[b] Middle East Technical University, Department of Electrical and Electronic Eng., Ankara, Turkey

ARTICLE INFO

Article history:
Received 15 February 2013
Received in revised form 14 September 2013

Keywords:
Dynamic analysis
Rigid multi-body dynamics
Stabilization platform
Friction
Simulation
Model validation

ABSTRACT

Typical operating conditions for mobile sensor systems, and in particular mobile robots, exhibit a wide range of mechanical disturbances due their ego-motion. Sensor systems mounted on these mobile platforms often suffer to varying degrees from these disturbances. The quality of acquired data is degraded as a result. For instance, the quality of captured video frames from an onboard camera greatly depends on the angular velocity of the body on which the camera is mounted. Motion blur degradation results if large angular motions are present. In order to compensate for such disturbances, stabilization platforms are used. A common approach is measuring body movements using inertial sensors and attempting their cancellation with actuators and control systems. Design of high performance control systems often requires analytical system models. In this article, a planar stabilization platform is considered, to develop and study its kinematic and simple-to-complex dynamic model. The mathematical derivation of the model is presented with and without neglect of the actuator mass components as well as friction effects. This is followed by the comparative validation of these model alternatives against a realistic numerical model fitted to physical experimental data. The results demonstrate that the analytical model, in particular with the actuator mass and friction components included, provides a high degree of fit to the actual behavior.

1. Introduction

Many applications involve platforms that are subjected to either external motion disturbances or disturbances that are due to the ego-motion of the platform. Typical examples are provided by mobile sensor platforms, and in particular mobile robots carrying a variety of sensors. Legged robots are examples that exhibit more severe motion disturbances due to the impulsive nature of legged locomotion. Many sensors are sensitive to such disturbances either from a vibration/reliability perspective or in relation to the quality of the collected data. For instance, image capture devices such as video cameras are sensitive to such disturbances because camera motion exceeding camera dependent limits may cause image degradations such as *motion blur* [1]. Utilization of stabilization platforms that use high performance actuators combined with control algorithms is the common approach for compensating for these motion disturbances and improving the data collection process. Here, the sensor(s) are placed on top of a platform that is actively moved in order the cancel the effect of the disturbing motion.

☆ This work was supported by TUBITAK under project code 110E120.

* Corresponding author. Tel.: +90 533 7363220.
E-mail addresses: babak.rohani@metu.edu.tr (B. Rohani), yigit@metu.edu.tr (Y. Yazicioglu), mehmet.odtu@gmail.com, memutlu@metu.edu.tr (M. Mutlu), orkunogucu@gmail.com (O. Ogucu), emrea@eee.metu.edu.tr (E. Akgul), afsars@metu.edu.tr (A. Saranli).

0377-0427/$ – see front matter © 2013 Elsevier B.V. All rights reserved.
http://dx.doi.org/10.1016/j.cam.2013.10.018

Besides those in mobile robotics, there are many applications for stabilized platforms. For example, cameras mounted on aircraft are also subjected to large disturbances. However, with the use of stabilization platforms they can capture sharp images without any motion blur even for low altitude flight under turbulent air conditions [2]. In an underwater suspended work platform, an actively controlled stabilization system enables a stable working base even though the underwater work platform is subjected to large water currents [3]. For stabilization platforms one of the most widely used mechanisms is the Stewart Platform.

The development in platform stabilization technology is driven primarily by accelerating developments in sensor technologies such as those of inertial sensors using microelectromechanical systems (MEMS) [4], low cost precision machinery [5], digital video signal processing methods and algorithms [6] as well as power electronics and servo drive technologies [7]. For example, the small scale mechanism presented in the present work has been made possible by the availability of very small size brushless linear motors.

Research for defense systems has always been a driving factor. Advanced defense systems based on inertial sensors widely utilized stabilized platforms, but high cost sensors limited the adoption of these technologies for more widespread applications. The US Navy, for example, used the quartz tuning fork gyroscope to develop the ship based satellite antenna stabilization system [8–10].

On the methods side for camera based applications, stabilization approaches have been studied by researchers for decades, and many video stabilization schemes have been proposed. These can be classified into two broad categories [11]: (1) image processing based (algorithmic) stabilization and (2) mechanical (motion) based video stabilization. The former class focuses on processing corrupted image frames either individually or in sequence to recover image data suitable for the given application, while the latter approach (the focus of the present paper) is based on electromechanical design coupled with automatic control to physically stabilize the camera platform.

Firstly on the algorithmic side, some examples can be discussed. For example, a real-time smoothing methodology for the stabilization of videos captured from small robotic helicopter platforms is introduced in [12]. It uses a Lucas–Kanade feature tracker to detect the regions and then estimate the transformation between two consecutive frames. A fast video stabilization algorithm presented in [13] uses a circular block to search for and match the key places. A dual-pass video stabilization system in [14] uses an iterative method for global motion estimation and an adaptive window smoothing for the intentional motion estimation. This method is only for off-line processing of video stabilization. The processing speed can reach 25 fps. A method is proposed in [15] for removing the camera shake in the video sequence and reconstructing a stabilized video sequence with good visual quality. Algorithmic approaches to image stabilization are not the focus of the present paper and hence will not be further discussed.

Motion control based approaches for improving the camera image stream are based on sensing the motion disturbances affecting the camera and using advanced automatic control approaches coupled with actuators to compensate/cancel these disturbances. As a result, a camera which experiences only the residual disturbances results in a major improvement in image data. Cancellation of motion blur is a very important application example. Most commonly, the design of control systems for such motion control requires an analytic platform model. Such models can be linearized around operating points to design high performance linear and optimal controllers such as the linear–quadratic regulator (LQR) [16]. This fact strongly motivates the mathematical model developed in the present study.

Although different kinematic configurations can be designed in order to obtain a three-degree-of-freedom (DoF) angular stabilization of a camera platform, our focus is on parallel kinematic structure, an angular-only special case of the Stewart Platform [17]. This structure has a number of advantages: its design is homogeneous (three identical actuators), it is mechanically simpler than a closed-chain (gimbal type) structure and, finally, the study of its planar special case is a major step in modeling the 3-DoF general form. The contribution of the present paper is twofold. Firstly, a mathematical model of the planar case is derived from first principles using the Lagrangian formulation. This involved a both kinematic and dynamic formulation. The contribution of the masses of the motor body and motor shaft are compared with that of the platform, studied in the model. Secondly, the effect of friction is studied by explicit addition to the model. The mathematical model is validated using a two-stage experimental approach.

The paper is organized as follows. We start in Section 2 with the kinematic analysis of the platform. This is followed by Sections 3 and 4 where the dynamic motion analysis of the platform is presented for two different approximations. Section 5 presents the experimental results composed, in sequence, of the experimental validation of the kinematic model, the experimental validation of the baseline numerical dynamic model and the validation of the analytical dynamic model. The paper concludes with our observations.

2. Kinematic analysis

In Fig. 1(a) and (b) the stabilization platform in planar motion, together with body fixed reference frames, is shown.

The relation between the input motor shaft displacement (S) and the output platform angular displacement (θ) is the fundamental kinematic relationship that should be determined as a first step in the analysis. The closed kinematic chain structure requires that we have the vector relation

$$\overrightarrow{OA} + \overrightarrow{AB} = \overrightarrow{OE} + \overrightarrow{ED} + \overrightarrow{DC} + \overrightarrow{CB}, \tag{1}$$

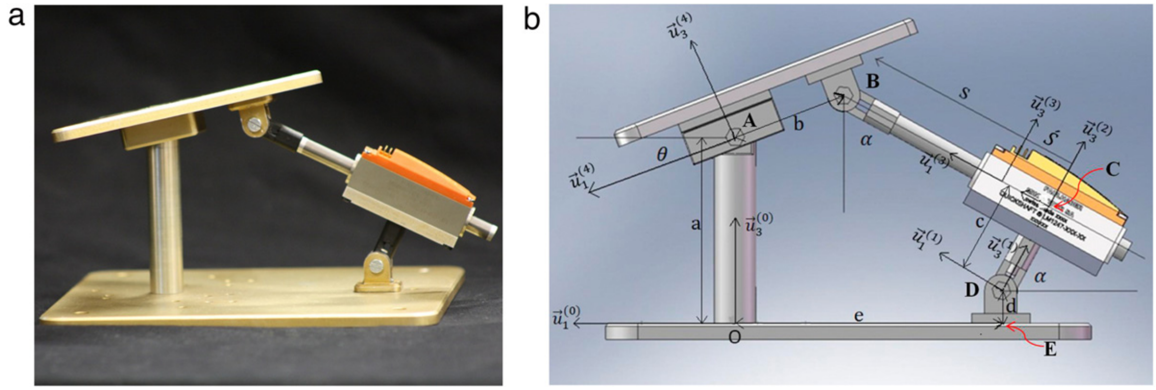

Fig. 1. Planar stabilization platform. (a) Physical experimental setup; (b) solid model with axis definitions and unit vectors.

which is known as the loop closure equation (LCE) of the mechanism. This can also be written in terms of the coordinate frame unit vectors as

$$a\vec{j} + b\cos(\theta)\vec{i} + b\sin(\theta)\vec{j} = e\vec{i} + d\vec{j} + c\cos(\alpha)\vec{i} + c\sin\alpha\vec{j} + S\cos(\alpha)\vec{j} - S\sin(\alpha)\vec{i}. \tag{2}$$

Eq. (2) can be transformed into two scalar equations given by

$$b\cos(\theta) = e + c\cos(\alpha) - S\sin(\alpha), \tag{3}$$

$$a + b\sin(\theta) = d + c\sin(\alpha) + S\cos(\alpha). \tag{4}$$

We define the three terms

$$A = e^2 - c^2 + (a-d)^2 + b^2, \tag{5}$$

$$B = 2eb, \tag{6}$$

$$C = 2b(a-d). \tag{7}$$

Then by rearranging, squaring and adding Eqs. (3) and (4), we obtain

$$S = \sigma\sqrt{A - B\cos(\theta) + C\sin(\theta)}, \tag{8}$$

where we have $\sigma = \pm 1$. Of these two possibilities, $\sigma = -1$ is impossible because there is a joint restriction, leaving with the final kinematic relationship between S and θ as

$$S = \sqrt{A - B\cos(\theta) + C\sin(\theta)}. \tag{9}$$

Also, the relationship between the output angular displacement θ and actuator angle α is obtained from Eqs. (3) and (4) by calculating the sine and cosine of α as

$$\sin\alpha = \frac{-Sb\cos\theta + ac + bc\sin\theta + Se - dc}{S^2 + c^2}, \tag{10}$$

$$\cos\alpha = \frac{bc\cos\theta + aS + bS\sin\theta - ec - dS}{S^2 + c^2}. \tag{11}$$

Another relationship that will be useful later in the dynamic analysis relates the velocities of the actuator angle α and the output platform angle θ, and also the velocities of the motor shaft displacements S and the output platform angle θ. From Eqs. (3) and (4), a lengthy derivation leads to

$$\begin{bmatrix} (c\sin\alpha + S\cos\alpha) & \sin\alpha \\ (c\cos\alpha - S\sin\alpha) & \cos\alpha \end{bmatrix} \begin{bmatrix} \dot{\alpha} \\ \dot{S} \end{bmatrix} = \begin{bmatrix} b\dot{\theta}\sin(\theta) \\ b\dot{\theta}\cos(\theta) \end{bmatrix}. \tag{12}$$

3. Dynamic analysis using the Lagrangian formulation (one body)

In this and the following sections, we assume that the input to the system is a force exerted by the motor shaft and determine the dynamic response of the platform output angle. The Lagrangian approach is used for deriving the equations of motion (EoM) for the platform. As a first approximation, only the mass properties of the stabilized platform are considered in the formulation.

For our mechanism, we have the system DoF $=1$ and the single generalized coordinate is θ. We have the platform angular velocity given by[1]

$$\vec{\omega}_{\text{platform}} = \dot{\theta}\vec{u}_2^{(4)}. \tag{13}$$

In the following formulation, the dyadic notation is used in order to develop a reference frame independent vector formulation. The moment of inertia dyadic of the platform with respect to the mass center is given by

$$\begin{aligned}\check{J}_{\text{platform}} = \check{J}_{\text{p}} = {} & J_{\text{p11}}\vec{u}_1^{(4)}\vec{u}_1^{(4)} + J_{\text{p12}}\vec{u}_1^{(4)}\vec{u}_2^{(4)} + J_{\text{p13}}\vec{u}_1^{(4)}\vec{u}_3^{(4)} + J_{\text{p12}}\vec{u}_2^{(4)}\vec{u}_1^{(4)} \\ & + J_{\text{p22}}\vec{u}_2^{(4)}\vec{u}_2^{(4)} + J_{\text{p23}}\vec{u}_2^{(4)}\vec{u}_3^{(4)} + J_{\text{p13}}\vec{u}_3^{(4)}\vec{u}_1^{(4)} + J_{\text{p23}}\vec{u}_3^{(4)}\vec{u}_2^{(4)} + J_{\text{p33}}\vec{u}_3^{(4)}\vec{u}_3^{(4)}.\end{aligned} \tag{14}$$

The kinetic energy equation can then be written and simplified as

$$K = \frac{1}{2}\vec{\omega}_{\text{p}} \cdot \check{J}_{\text{p}} \cdot \vec{\omega}_{\text{p}} = \frac{1}{2}J_{\text{p22}}\dot{\theta}^2. \tag{15}$$

The virtual work expression is given by

$$\delta W = Q_\theta \delta_\theta = F\delta_S, \tag{16}$$

where F is the actuating force applied by the linear motor. Now, δ_S is written in the δ_θ coordinates. From (9), we have

$$\delta_S = \frac{B\sin(\theta) + C\cos(\theta)}{2S}\delta_\theta. \tag{17}$$

Inserting Eq. (17) into (16), we obtain

$$\delta W = F\frac{B\sin(\theta) + C\cos(\theta)}{2S}\delta_\theta. \tag{18}$$

By comparing Eqs. (16) and (18), one can obtain

$$Q_\theta = F\frac{B\sin(\theta) + C\cos(\theta)}{2S}. \tag{19}$$

Finally, we define the generalized momenta as given by

$$P_\theta = \frac{\partial K}{\partial \dot{\theta}} = J_{\text{p22}}\dot{\theta}. \tag{20}$$

In the analysis, friction forces between mechanical parts are also modeled. The Rayleigh dissipation function given by

$$D = \frac{1}{2}\sum_{i=1}^{l} c_i V_{\text{rel},i}^2 \tag{21}$$

can be used for modeling the viscous friction [18,19].

The platform considered has three revolute joints and a prismatic joint. The viscous friction model is used for all joints. The first one is the revolute joint which is connecting the motor body to the base, and its coefficient is denoted as c_1. The second one is the revolute joint between the platform and the motor shaft, and its coefficient is c_2. The third one is the revolute joint between the stabilization platform and the main fixed column on the base, with the coefficient given by c_3. The final one is the prismatic joint between the motor shaft and motor body, with the coefficient c_4. Therefore, the total dissipation function becomes

$$D = \frac{1}{2}c_1\dot{\alpha}^2 + \frac{1}{2}c_2\dot{\alpha}^2 + \frac{1}{2}c_3\dot{\theta}^2 + \frac{1}{2}c_4\dot{S}^2. \tag{22}$$

Taking the derivative of Eq. (22) with respect to $\dot{\theta}$ and substituting $\dot{S}$ and $\dot{\alpha}$ with $\dot{\theta}$ by using Eq. (12), the dissipation function expression becomes

$$\frac{\partial D}{\partial \dot{\theta}} = \frac{\partial D}{\partial \dot{\theta}} + \frac{\partial D}{\partial \dot{\alpha}}\frac{\partial \dot{\alpha}}{\partial \dot{\theta}} + \frac{\partial D}{\partial \dot{S}}\frac{\partial \dot{S}}{\partial \dot{\theta}} \tag{23}$$

$$\frac{\partial D}{\partial \dot{\theta}} = c_3\dot{\theta} + (c_1\dot{\alpha} + c_2\dot{\alpha})\frac{\partial \dot{\alpha}}{\partial \dot{\theta}} + (c_4\dot{S})\frac{\partial \dot{S}}{\partial \dot{\theta}}. \tag{24}$$

In Eq. (24), $\frac{\partial \dot{\alpha}}{\partial \dot{\theta}}$ and $\frac{\partial \dot{S}}{\partial \dot{\theta}}$ were obtained from Eq. (12).

For the one-body formulation, only the mass of the platform is considered and its center of mass (CoM) coincides with the joint. Therefore the potential energy change due to platform angle change is zero. Hence we have $\frac{\partial U}{\partial \theta} = 0$ and the Lagrange

[1] The superscript in unit vectors shows the reference frame and the subscript denotes the axes of Cartesian coordinates, e.g. 2 corresponds to the y axis.

equation becomes

$$\dot{P}_\theta - \frac{\partial K}{\partial \theta} + \frac{\partial D}{\partial \dot{\theta}} + \frac{\partial U}{\partial \theta} = Q_\theta. \tag{25}$$

The equation of motion is then obtained as

$$J_{p22}\ddot{\theta} = F\frac{B\sin(\theta) + C\cos(\theta)}{2S} - \left(c_3\dot{\theta} + (c_1\dot{\alpha} + c_2\dot{\alpha})\frac{\partial \dot{\alpha}}{\partial \dot{\theta}} + (c_4\dot{S})\frac{\partial \dot{S}}{\partial \dot{\theta}}\right). \tag{26}$$

4. Dynamic analysis using the Lagrangian formulation (three bodies)

For deriving the Lagrange equation for the three-body case, the CoM velocity and the CoM angular velocity of the motor, motor shaft and platform should be considered. In this case the kinetic and potential energies of the CoMs of the three bodies are calculated.

From Fig. 1(b), the displacement of the CoM of the motor can be obtained as follows:

$$\vec{r}_m = \vec{r}_{m/o} = \overrightarrow{OC} = \overrightarrow{OE} + \overrightarrow{ED} + \overrightarrow{DC}, \tag{27}$$

$$\vec{r}_m = -e\vec{u}_1^{(0)} + d\vec{u}_3^{(0)} + c\vec{u}_3^{(1)}. \tag{28}$$

The displacement of the CoM of the motor in matrix notation with respect to the platform base fixed reference (inertial) frame is given by

$$\bar{r}_m^{(0)} = -e\bar{u}_1^{(0/0)} + d\bar{u}_3^{(0/0)} + c\bar{u}_3^{(1/0)}, \tag{29}$$

$$\bar{r}_m^{(0)} = -e\bar{u}_1 + d\bar{u}_3 + c\hat{c}^{(0,1)}\bar{u}_3, \tag{30}$$

where $\hat{c}^{(0,1)}$ denotes the rotation matrix between reference frames (0) and (1) utilizing the rotational frame base (RFB) sequence. It is given by $\hat{c}^{(0,1)} = e^{\tilde{u}_2(\frac{\pi}{2}-\alpha)}$ as a rotation about $\vec{u}_2$. Hence, we have

$$\bar{r}_m^{(0)} = -e\bar{u}_1 + d\bar{u}_3 + ce^{\tilde{u}_2(\frac{\pi}{2}-\alpha)}\bar{u}_3. \tag{31}$$

Expanding the last term, we further obtain

$$\bar{r}_m^{(0)} = -e\bar{u}_1 + d\bar{u}_3 + c\left[\bar{u}_3\cos\left(\frac{\pi}{2} - \alpha\right) + \bar{u}_1\sin\left(\frac{\pi}{2} - \alpha\right)\right], \tag{32}$$

$$\bar{r}_m^{(0)} = -e\bar{u}_1 + d\bar{u}_3 + c[\bar{u}_3\sin(\alpha) + \bar{u}_1\cos(\alpha)], \tag{33}$$

which, in vector notation with respect to the base frame, becomes

$$\vec{r}_m = \vec{u}_1^{(0)}(c\cos(\alpha) - e) + \vec{u}_3^{(0)}(c\sin(\alpha) + d). \tag{34}$$

The velocity of the motor CoM can similarly be expressed as follows:

$$\vec{v}_m = \vec{v}_{m/F_0(o)} = D_0\vec{r}_m = \vec{u}_1^{(0)}(-c\dot{\alpha}\sin(\alpha)) + \vec{u}_3^{(0)}(c\dot{\alpha}\cos(\alpha)). \tag{35}$$

For obtaining the equation of motion, the scalar expression for the velocity is needed. We have

$$|\vec{v}_m|^2 = (c\dot{\alpha}\sin(\alpha))^2 + (c\dot{\alpha}\cos(\alpha))^2, \tag{36}$$

$$|\vec{v}_m|^2 = c^2\dot{a}^2. \tag{37}$$

The angular velocity of the motor is obtained as

$$\vec{\omega}_m = \vec{\omega}_{1/0} = -\dot{\alpha}\vec{u}_2^{(1)} = -\dot{\alpha}\vec{u}_2^{(2)}. \tag{38}$$

The reference frame (2) is fixed to the CoM of the motor as illustrated in Fig. 1(b). The motor moment of inertia dyadics with respect to the CoM are

$$\begin{aligned}\check{J}_m \;=\; & J_{m11}\vec{u}_1^{(2)}\vec{u}_1^{(2)} + J_{m12}\vec{u}_1^{(2)}\vec{u}_2^{(2)} + J_{m13}\vec{u}_1^{(2)}\vec{u}_3^{(2)} + J_{m12}\vec{u}_2^{(2)}\vec{u}_1^{(2)} + J_{m22}\vec{u}_2^{(2)}\vec{u}_2^{(2)} \\ & + J_{m23}\vec{u}_2^{(2)}\vec{u}_3^{(2)} + J_{m13}\vec{u}_3^{(2)}\vec{u}_1^{(2)} + J_{m23}\vec{u}_3^{(2)}\vec{u}_2^{(2)} + J_{m33}\vec{u}_3^{(2)}\vec{u}_3^{(2)}.\end{aligned} \tag{39}$$

$$\vec{\omega}_m \cdot \check{J}_m \cdot \vec{\omega}_m = J_{m22}\dot{\alpha}^2. \tag{40}$$

In order to calculate the CoM velocity and angular velocity of the motor shaft we may proceed as follows. From Fig. 1(b) the displacement of the CoM is given by

$$\vec{r}_{sh} = \vec{r}_{\grave{B}/O} = \overrightarrow{O\grave{B}} = \overrightarrow{OE} + \overrightarrow{ED} + \overrightarrow{DC} + \overrightarrow{C\grave{B}}. \tag{41}$$

$$\vec{r}_{sh} = -e\vec{u}_1^{(0)} + d\vec{u}_3^{(0)} + c\vec{u}_3^{(1)} + \grave{S}\vec{u}_1^{(1)} \tag{42}$$

where S is the current actuator length and $\grave{S}$ is the change of the actuator length from its rest position, given as

$$\grave{S} = S - S_0 \tag{43}$$

where S_0 is the initial position of the shaft.

Similarly, the scalar magnitude of the shaft velocity is

$$\vec{v}_{sh}^2 = (c\dot{\alpha} - \dot{S})^2 + (S - S_0)^2\dot{\alpha}^2. \tag{44}$$

The angular velocity of the motor shaft is obtained as

$$\vec{\omega}_m = \vec{\omega}_{1/0} = -\dot{\alpha}\vec{u}_2^{(1)} = -\dot{\alpha}\vec{u}_2^{(2)} = -\dot{\alpha}\vec{u}_2^{(3)}. \tag{45}$$

The reference frame (3) is fixed to the motor shaft CoM as in Fig. 1(b). The motor moment of inertia dyadics with respect to this CoM are

$$\begin{aligned}\check{J}_{sh} &= J_{sh11}\vec{u}_1^{(3)}\vec{u}_1^{(3)} + J_{sh12}\vec{u}_1^{(3)}\vec{u}_2^{(3)} + J_{sh13}\vec{u}_1^{(3)}\vec{u}_3^{(3)} + J_{sh12}\vec{u}_2^{(3)}\vec{u}_1^{(3)} + J_{sh22}\vec{u}_2^{(3)}\vec{u}_2^{(3)}\\ &\quad + J_{sh23}\vec{u}_2^{(3)}\vec{u}_3^{(3)} + J_{sh13}\vec{u}_3^{(3)}\vec{u}_1^{(3)} + J_{sh23}\vec{u}_3^{(3)}\vec{u}_2^{(3)} + J_{sh33}\vec{u}_3^{(3)}\vec{u}_3^{(3)}\end{aligned} \tag{46}$$

$$\vec{\omega}_{sh} \cdot \check{J}_{sh} = -\dot{\alpha}J_{sh12}\vec{u}_1^{(3)} - \dot{\alpha}J_{sh22}\vec{u}_2^{(3)} - \dot{\alpha}J_{sh23}\vec{u}_3^{(3)}. \tag{47}$$

$$\vec{\omega}_{sh} \cdot \check{J}_{sh} \cdot \vec{\omega}_{sh} = J_{sh22}\dot{\alpha}^2. \tag{48}$$

The kinetic energy of the system is given by the equation

$$K = \frac{1}{2}m_m|\vec{v}_m|^2 + \frac{1}{2}\vec{\omega}_m \cdot \check{J}_m \cdot \vec{\omega}_m + \frac{1}{2}m_{sh}|\vec{v}_{sh}|^2 + \frac{1}{2}\vec{\omega}_{sh} \cdot \check{J}_{sh} \cdot \vec{\omega}_{sh} + \frac{1}{2}m_{\mathrm{p}}|\vec{v}_{\mathrm{p}}|^2 + \frac{1}{2}\vec{\omega}_{\mathrm{p}} \cdot \check{J}_{\mathrm{p}} \cdot \vec{\omega}_{\mathrm{p}}. \tag{49}$$

Inserting Eqs. (37), (40), (44) and (48) into (49) and also using the simplification in Eq. (15), we obtain

$$K = \frac{1}{2}m_m c^2\dot{\alpha}^2 + \frac{1}{2}J_{m22}\dot{\alpha}^2 + \frac{1}{2}m_{sh}[(c\dot{\alpha} - \dot{S})^2 + (S - S_0)^2\dot{\alpha}^2] + \frac{1}{2}J_{sh22}\dot{\alpha}^2 + \frac{1}{2}J_{\mathrm{p}22}\dot{\theta}^2. \tag{50}$$

Now, we define generalized momenta as

$$P_\theta = \frac{\partial K}{\partial\dot{\theta}} + \frac{\partial K}{\partial\dot{\alpha}}\frac{\partial\dot{\alpha}}{\partial\dot{\theta}} + \frac{\partial K}{\partial\dot{S}}\frac{\partial\dot{S}}{\partial\dot{\theta}}, \tag{51}$$

and from Eq. (12), we obtain

$$P_\theta = J_{\mathrm{p}22}\dot{\theta} + [m_m c^2\dot{\alpha} + J_{m22}\dot{\alpha} + m_{sh}c(c\dot{\alpha} - \dot{S}) + m_{sh}(S - S_0)^2\dot{\alpha} + J_{sh22}\dot{\alpha}]\frac{\partial\dot{\alpha}}{\partial\dot{\theta}} + [-m_{sh}(c\dot{\alpha} - \dot{S})]\frac{\partial\dot{S}}{\partial\dot{\theta}}. \tag{52}$$

The potential energy equation becomes

$$U = (d + c\sin(\alpha))m_m g + [d + c\sin(\alpha) + (S - S_0)\cos(\alpha)]m_{sh}g \tag{53}$$

while its partial derivative is

$$\frac{\partial U}{\partial\theta} = \frac{\partial U}{\partial\alpha}\frac{\partial\alpha}{\partial\theta} + \frac{\partial U}{\partial S}\frac{\partial S}{\partial\theta}. \tag{54}$$

Hence, we have

$$\frac{\partial U}{\partial\theta} = [cm_m g\cos(\alpha) + cm_{sh}g\cos(\alpha) - (S - S_0)m_{sh}g\sin(\alpha)]\frac{\partial\alpha}{\partial\theta} + m_{sh}g\cos(\alpha)\frac{\partial S}{\partial\theta}. \tag{55}$$

The friction (dissipation force) expression is the same as for one-body analysis. The Lagrange equation is given by

$$\dot{P}_\theta - \frac{\partial K}{\partial\theta} + \frac{\partial D}{\partial\dot{\theta}} + \frac{\partial U}{\partial\theta} = Q_\theta. \tag{56}$$

By substituting the derived Lagrangian terms into Eq. (56), the equation of motion is obtained in the form of

$$\ddot{\theta} = f(\theta, \dot{\theta}, F, t). \tag{57}$$

5. Experimental and simulation results

In this section, we present simulation and experimental results, to validate the analytical model developed, and comparatively present results with respect to the contribution of the secondary masses in the system as well as friction. Since our physical experimental setup does not have the ability to apply controlled forces, nor a means of measuring motor shaft force, we needed to follow a two-stage experimental approach. In stage 1, we build a numerical model in Matlab-SimMechanics

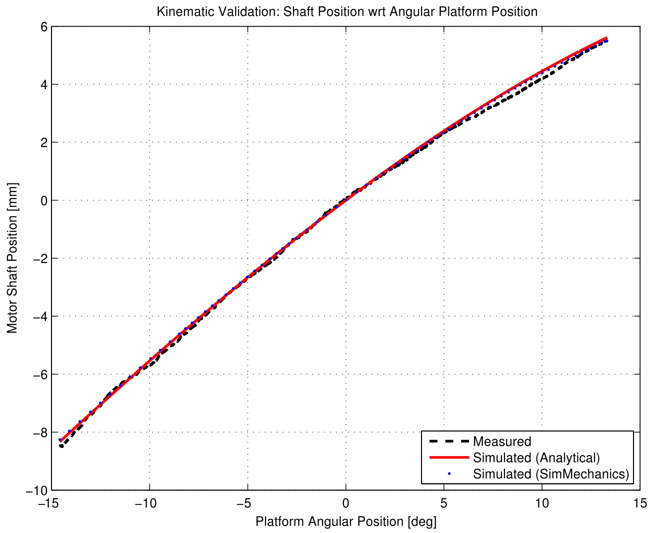

Fig. 2. The validation of the analytical kinematic model against the SimMechanics numerical model and the physical platform setup.

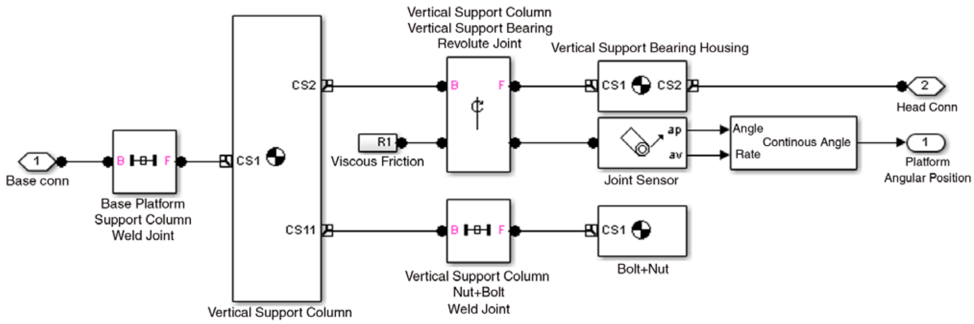

Fig. 3. A sample section (central support pillar) of the SimMechanics intermediate numerical model.

and validate it using physical experiments with the platform setup. Here, gravity is used alone as a known driving force for the platform. Once we have the intermediate numerical model as a baseline, in stage 2 it is then used as a basis for validating the analytical model itself. At this stage, being in a simulation gives us the means of exciting the two models using known force inputs, and observing and comparing the behaviors.

5.1. *Validation of the kinematic model*

For the kinematic analysis, it was possible to fully validate the analytical model against the physical setup and this is what the first set of results presented here show. For this, the platform was driven in position controlled mode, very slowly, for a range of shaft positions and resulting platform angles. The same shaft position samples were also used as an input to the analytical model as well as the intermediate baseline numerical model. The results for these three cases are comparatively illustrated in Fig. 2, where the close overlap between the two sets of results is apparent. These results also include the overlap of the SimMechanics based intermediate numerical model that will be described in the following section.

5.2. *The baseline numerical model using Matlab-SimMechanics*

As a first stage of the validation of the analytical dynamic model, we have developed an intermediate numerical model in Matlab-Simulink, that closely models the physical setup using an interconnection of mechanical components. SimMechanics has been shown to generate accurate dynamic models of complex mechanical systems [20]. A section of our numerical model in SimMechanics is illustrated in Fig. 3. The model is hierarchical and is composed of other sub-blocks. For both the analytical model and this intermediate numerical model, the model parameters are derived from the actual physical system and the source solid model design files. These are given in Table 1.

Nevertheless, this numerical model was cross-validated with the actual physical system through a system identification experiment. The viscous friction parameters of the intermediate numerical model were also the output for the experiment as well as the observation of the overlap between the model and the physical system. In the experiment, the platform was

Table 1
Model and simulation parameters obtained from the physical setup and solid model design files.

Parameter	Value	Unit	Parameter	Value	Unit
a	57.48	mm	J_{m22}	$11.1857 * 10^{-6}$	kg m^2
b	35.99	mm	m_{sh}	19.1	g
c	29.55	mm	J_{sh22}	$12.94578 * 10^{-6}$	kg m^2
d	10.03	mm	c_1	1.5260e−06	N m s/°
e	81.64	mm	c_2	1.5260e−06	N m s/°
m_p	92.33	g	c_3	1.2543e−08	N m s/°
J_{p22}	$53.87012 * 10^{-6}$	kg m^2	c_4	8.9949e−06	N s/m
m_m	48.1	g			

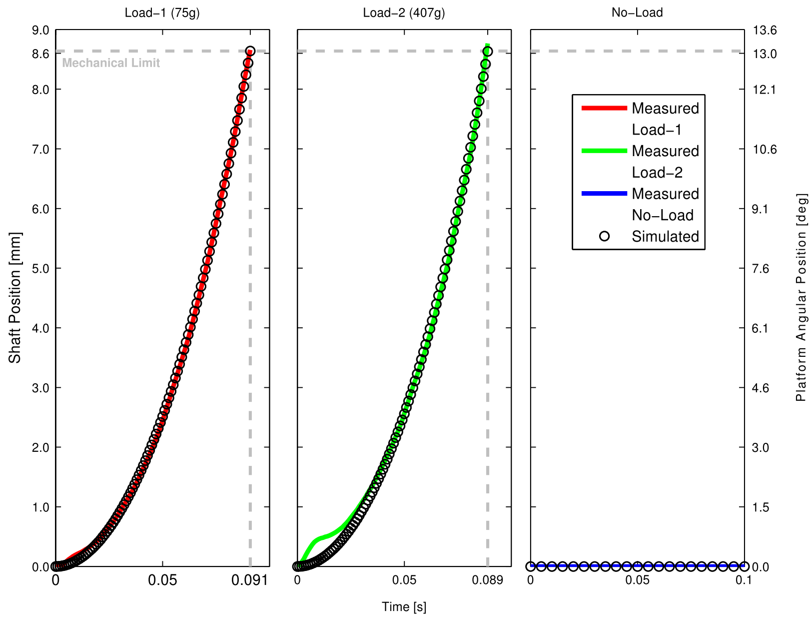

Fig. 4. Intermediate numerical model validation using gravitational fall experiments with the physical platform setup.

set to an initial angle where gravity would pull the platform into motion. Since the gravitational force is known, the same conditions could be applied both for the physical system and in the simulation. The result of the experiment is illustrated in Fig. 4. One may see that the intermediate numerical model built in SimMechanics closely approximates the physical system behavior, building confidence that one may use it as a baseline for the subsequent experimentation. The small deviation for the larger load may be attributed to the nonlinearity of physical friction that may result from higher loads on the joints.

5.3. Validation of the analytical dynamic platform model

Finally, it is possible to present the validation of the dynamic part of the analytical model which is the main mathematical contribution of the present paper. This is achieved by making use of the intermediate numerical SimMechanics model as a baseline for validating the behavior of the analytical model under gravity and known force excitation as well as the presence or absence of a viscous friction component. This final set of experiments is conducted exclusively in the simulation environment. The analytical model (the final set of equations of motion) is numerically integrated while Simulink integrates the intermediate SimMechanics model. The first two experiments are conducted with a constant force applied first in the positive direction from the negative limit of the mechanism and then in the negative direction from the positive angular limit. The simulation is run until the final platform is $\theta = 25^\circ$ (way beyond the mechanism limit of about $\theta = 13^\circ$). Fig. 5(a) and (b) illustrate superimposed plots of the analytical model and the baseline SimMechanics numerical model. In this experiment, (a) illustrates the case where gravity is neglected and (b) the case where gravity is present. Similarly, the case with the addition of the viscous friction model is given in Fig. 6. Although we have small friction values in the system, the experiment with the addition of the friction model shows that the presence of friction further reduces the mismatch between the analytical model and intermediate numerical model outputs.

For another comparative experiment, Fig. 7 illustrates a comparison of the one-body and three-body approximations in the model, and hence the effect of neglecting or including the masses and inertias of the motor shaft and motor body. This experiment is conducted with constant force and gravity as input. The friction is taken as zero for this experiment. From the

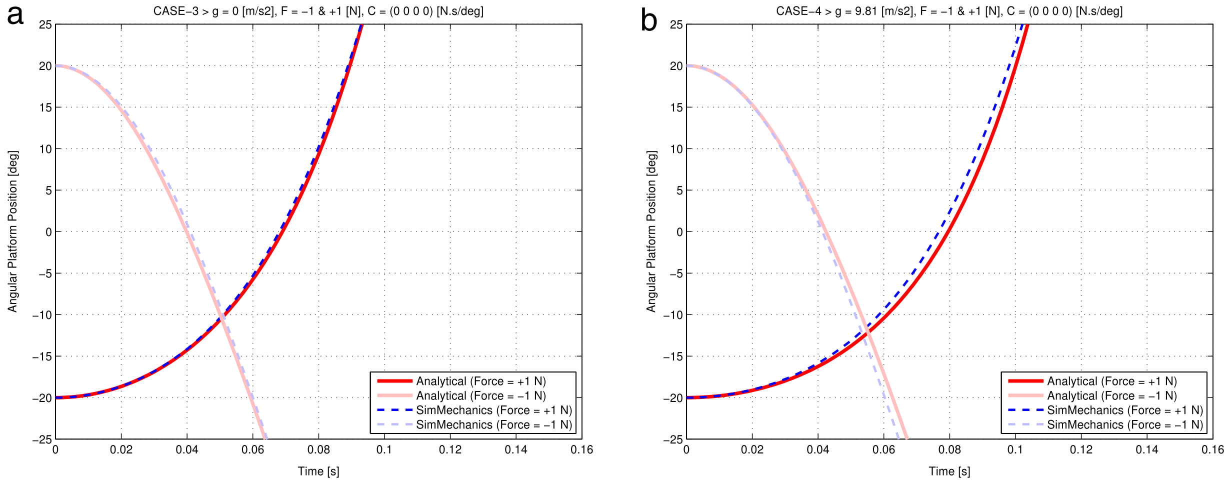

Fig. 5. Validation of the analytical model with constant force input. The viscous friction coefficient is zero. (a) Gravity is neglected. (b) Gravity is present.

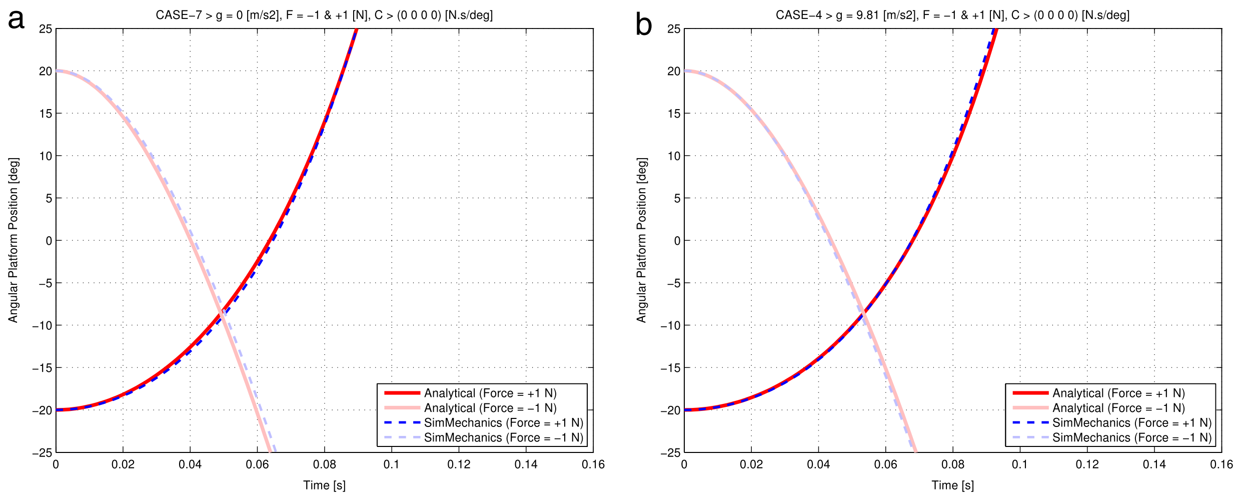

Fig. 6. Validation of the analytical model with constant force input. The viscous friction is nonzero. (a) Gravity is neglected. (b) Gravity is present.

figure, it can be observed that the one-body approximation significantly deviates from the three-body approximation, and hence from the true behavior of the physical system.

Collectively from these results, one may draw a number of conclusions. The analytical model composed of the nonlinear equations of motion for the system approximates well a fully numerical model generated by SimMechanics, which itself was validated against the physical system. There is a small amount of discrepancy between the models, which particularly manifests itself under the gravitational effect, leading to the conclusion that very small inaccuracies in the assumed mass properties as well as the homogeneous mass distribution assumption in the analytical model generate some mismatch. This is an expected result. We may also observe that errors due to the numerical integration process necessary for simulating the time responses contribute to the mismatch. Finally, the mismatch accumulates over time when the models are integrated numerically for a long period. Nevertheless, there is a reasonable confidence that the analytical model is sound and can model the system considered fairly well.

6. Conclusion

In this work, an analytic model is developed for a linear-motor actuated planar stabilization platform using the Lagrangian formulation. The model of the designed platform is studied for the one-body and three-body approximations and with the inclusion/exclusion of a viscous friction model. The model is experimentally validated using a system identification approach based on physical experiments. Physical experiments are directly used for validating the kinematic part of the model while a two-stage approach is required for the dynamic part, where an intermediate SimMechanics based numerical model is used. The experimental results, both physical and simulation based, have shown that the analytical model is sound with some small approximation errors. The small mismatch is shown to be mostly present when the gravitational input is nonzero.

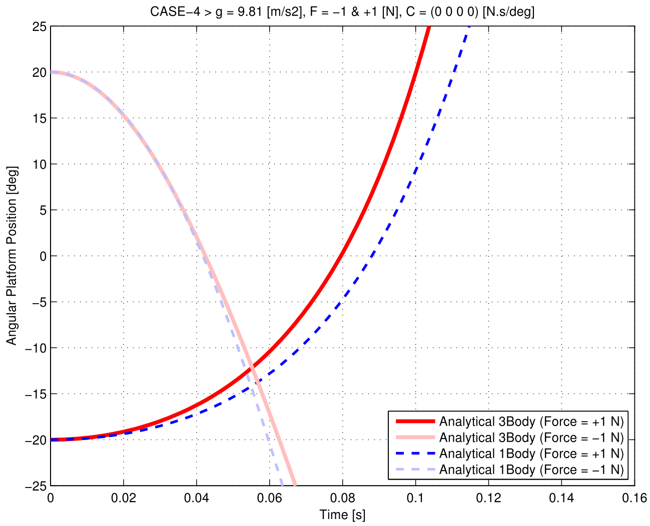

Fig. 7. The mismatch between the one-body and three-body analytic model approximations.

Overall, the model is accurate and is being used for developing control policies for regulating the platform angle and angular velocity.

References

[1] S. Nayar, M. Ben-Ezra, Motion-based motion deblurring, IEEE Transactions on Pattern Analysis and Machine Intelligence 26 (6) (2004) 689–698. http://dx.doi.org/10.1109/TPAMI.2004.1.

[2] M. Baumker, F.-J. Heimes, H. Hahn, W. Klier, R. Brechtken, T. Richter, Mathematical modeling, computer simulation, control and applications of a stabilized platform of an airborne sensor, in: Proceedings of the 19th International Society for Photogrammetry and Remote Sensing (ISPRS) Congress, The Netherlands, Amsterdam, 2001, pp. 278–286.

[3] R. Bostelman, J. Albus, Stability of an underwater work platform suspended from an unstable reference, in: Proceedings OCEANS'93. Engineering in Harmony with Ocean, Vol. 2, 1993, pp. II321–II325. http://dx.doi.org/10.1109/OCEANS.1993.326114.

[4] J. Hilkert, Inertially stabilized platform technology concepts and principles, IEEE Control Systems 28 (1) (2008) 26–46.

[5] E. Vermeulen, Real-time video stabilization for moving platforms, in: 21st Bristol UAV Systems Conference, 2007, pp. 3–4.

[6] P. Yang, Q. Li, Realization of TV guidance gyro stabilized platform and research of control algorithm, in: Proceedings of SPIE, vol. 6795, 2007, pp. 431–436.

[7] T. Lee, E. Koh, M. Loh, Stable adaptive control of multivariable servomechanisms, with application to a passive line-of-sight stabilization system, IEEE Transactions on Industrial Electronics 43 (1) (1996) 98–105.

[8] S.P. Wu, Three-axis stabilized platform control system development for mobile car, Master's Thesis, Nanjing University of Science and Technology, 2007.

[9] Z. Yang, The stability of vehicle antenna system design and engineering realization, Master's Thesis, Nanjing University of Science and Technology, 2004.

[10] L.B. Wang, Study of control system for stabilizing platform of mine-hunting sonar, Master's Thesis, Harbin Engineering University, 2007.

[11] Y. Shen, P. Guturu, T. Damarla, B. Buckles, K. Namuduri, Video stabilization using principal component analysis and scale invariant feature transform in particle filter framework, IEEE Transactions on Consumer Electronics 55 (3) (2009) 1714–1721.

[12] M. Vazquez, C. Chang, Real-time video smoothing for small RC helicopters, in: IEEE International Conference on Systems, Man and Cybernetics, 2009, SMC 2009, IEEE, 2009, pp. 4019–4024.

[13] H. Shen, Q. Pan, Y. Cheng, Y. Yu, Fast video stabilization algorithm for UAV, in: IEEE International Conference on Intelligent Computing and Intelligent Systems, 2009, Vol. 4, ICIS 2009, IEEE, 2009, pp. 542–546.

[14] P. Pan, A. Minagawa, J. Sun, Y. Hotta, S. Naoi, A dual pass video stabilization system using iterative motion estimation and adaptive motion smoothing, in: 2010 20th International Conference on Pattern Recognition (ICPR), IEEE, 2010, pp. 2298–2301.

[15] R. Hu, R. Shi, I.-f. Shen, W. Chen, Video stabilization using scale-invariant features, in: 11th International Conference Information Visualization, 2007, IV'07, IEEE, 2007, pp. 871–877.

[16] D. Kirk, Optimal control theory: an introduction, in: Dover Books on Engineering, Dover Publications, 2004.

[17] T. Zhao, J.S. Dai, Z. Huang, Geometric synthesis of spatial parallel manipulators with fewer than six degrees of freedom, Proceedings of the Institution of Mechanical Engineers, Part C (Journal of Mechanical Engineering Science) 216 (12) (2002) 1175–1185.

[18] F. Riewe, Nonconservative Lagrangian and Hamiltonian mechanics, Physical Review E 53 (1996) 1890–1899. http://dx.doi.org/10.1103/PhysRevE.53.1890.

[19] H. Goldstein, C. Poole, J. Safko, Classical Mechanics, 3e, Addison-Wesley Longman, Incorporated, 2002. Chapter 1.2.12.

[20] I. Besselink, H. Nijmeijer, A. Van der Knaap, W.J. Evers, Development and validation of a modular simulation model for commercial vehicles, International Journal of Heavy Vehicle Systems 16 (1–2) (2009) 132–153.